Atomic structure determination, electronic structure calculations and interpretation of electron transport properties of various 1/1-1/1-1/1 approximants

2002 J. Phys.: Condens. Matter 14 R767

(http://iopscience.iop.org/0953-8984/14/27/202)

INSTITUTE OF PHYSICS PUBLISHING JOURNAL OF PHYSICS: CONDENSED MATTER

J. Phys.: Condens. Matter **14** (2002) R767–R788 PII: S0953-8984(02)24799-2

TOPICAL REVIEW

Atomic structure determination, electronic structure calculations and interpretation of electron transport properties of various 1/1–1/1–1/1 approximants

Uichiro Mizutani[1], **Tsunehiro Takeuchi**[1] **and Hirokazu Sato**[2]

[1] Department of Crystalline Materials Science, Nagoya University, Furo-cho, Chikusa-ku, Nagoya 464-8603, Japan
[2] Aichi University of Education, Kariya-shi, Aichi-ken, 448-8542, Japan

Received 24 January 2002, in final form 30 May 2002
Published 28 June 2002
Online at stacks.iop.org/JPhysCM/14/R767

Abstract

The atomic structure of various 1/1–1/1–1/1 approximants has been extensively studied in the last decade to bridge the gap to that of the corresponding quasicrystal. Reliable information about electronic states in their valence bands has also been accumulated by using the atomic structure determined theoretically and experimentally. In this article, we have classified 1/1–1/1–1/1 approximants into three groups in terms of the structure type (P or F) and space group ($Im\bar{3}$ or $Pm\bar{3}$) and discussed characteristic features of both atomic and electronic structures of 1/1–1/1–1/1 approximants in each group. The electrical resistivity behaviour is then discussed on the basis of the atomic and electronic structures thus determined.

Contents

1. Introduction

Reliable determination of both the atomic and electronic structures of a quasicrystal is not feasible because of its possession of an infinitely large unit cell. To circumvent this difficulty, the determination of atomic structures of approximants is of great help, since conventional structure analysis for a crystal can be applied. As has been well established, the quasilattice of an icosahedral quasicrystal is constructed by appropriate cuts of a six-dimensional periodic lattice decorated with atomic hypersurfaces which are flat in the complementary space (see, for example, Yamamoto (1996)). Here the three-dimensional physical space is tilted so as to generate the Penrose lattice of two different unit cells. Likewise, approximant lattices of different orders can be constructed by rationalizing the slope so as to conform with a series of the Fibonacci ratios, $1/0$, $1/1$, $2/1$, $3/2 \ldots 1/\tau, \ldots$; τ is the golden mean given by $\tau = (1 + \sqrt{5})/2$. Indeed, the projection method allows for a more general notion of a quasicrystalline approximant (Krajcí *et al* 1995). Quasicrystals and their approximants are believed to be obtained by decorating the respective lattices with atoms or atom clusters.

The definition above for a quasicrystal and its approximant is rigorously made on the basis of the projection method from a higher-dimensional space. We discuss in this article the atomic structure and electronic properties of $1/1$–$1/1$–$1/1$ approximants synthesized experimentally. Here, the word 'approximant' will be used in a less strict sense. Rather than defining an approximant as a theoretically derived model structure projected from a higher-dimensional space, we assume that the formation of a realistic q/p–q/p–q/p approximant is justified when the following conditions are satisfied:

(1) a quasicrystalline phase exists near its composition in the same alloy system,
(2) the space group of $m\bar{3}$ holds and
(3) its lattice constant satisfies the relation $a_{q/p-q/p-q/p} = 2(p + q\tau)a_R/\sqrt{\tau^2 + 1}$, where a_R is the quasilattice constant of the corresponding quasicrystal.

We can experimentally identify the clusters in an approximant and consider this to motivate the assumption that they also exist in a quasicrystal. The clusters are certainly arranged in a periodic way in the former but in a quasiperiodic way in the latter. As its consequence, a similarity should exist in the short-range bonding character but the Fermi surface–Brillouin zone interaction characterizing a long-range order must be different between them. The effect of the short-range bonding character in the atomic cluster on one hand and of the long-range order on the other hand on the electronic structure and electron transport properties can be critically studied in the case of an approximant, since we can perform precise band calculations for the atomic structure determined experimentally. A sizeable pseudogap is known to be formed across the Fermi level as a result of a combination of these two effects.

Approximants of low orders, $1/0$–$1/0$–$1/0$, $1/1$–$1/1$–$1/1$ up to $2/1$–$2/1$–$2/1$, have been synthesized in a single-phase bulk form in many alloy systems. They are generally found in the vicinity of the composition where the thermally stable quasicrystalline phase exists. Among approximants of various orders, $1/1$–$1/1$–$1/1$ approximants have been most abundantly synthesized and studied in extended detail. We focus first on the experimental determination of the atomic structure of various $1/1$–$1/1$–$1/1$ approximants. For the sake of convenience, they are classified into three groups in terms of the space group and the structure type P or F, which has been used to classify quasicrystals in terms of the absence or presence of

the superlattice reflection lines in the diffraction spectra, respectively. The electronic structure can be calculated for the atomic structure thus determined and electron transport properties are interpreted on the basis of both the atomic and electronic structures thus obtained.

2. Atomic clusters in 1/1–1/1–1/1 approximants

Icosahedral quasicrystals have been divided into two families in terms of the cluster unit building up its structure: one described by the rhombic triacontahedron containing 44 atoms and the other by the Mackay icosahedron containing 54 atoms. The former is denoted as the RT-type or FK-type cluster, since its 1/1–1/1–1/1 approximant is known as the Frank–Kasper compound. The RT-type cluster is found in systems such as Al–Mg–X (X = Zn, Ag, Cu and Pd) and Al–Li–Cu quasicrystals and their approximants. The latter is denoted as the MI-type cluster and involves transition-metal (TM) elements as one of the major components. The MI-type atomic cluster is suited to describe the atomic structure of systems such as Al–Mn, Al–Cu–Fe, Al–Cu–Ru and Al–Pd–Re quasicrystals, in which the hybridization effect between 3p states of the Al atom and d states of the TM atom such as Mn, Fe, Ru and Re is known to be substantial (Trambly de Laissardiére *et al* 1995, Krajcí *et al* 1995, Takeuchi *et al* 1998, Belin-Ferré *et al* 2000, 2001, Mizutani *et al* 2001).

The atomic structure of both the RT- and MI-type clusters is illustrated in figure 1. In both cases, 12 atoms are located around a given lattice site to form an icosahedral cluster. The centre of the icosahedron thus formed is fully or partially filled with an atom or more frequently completely vacant. These 12 atoms are said to constitute the first shell of the cluster. There exist 20 triangular faces on the icosahedron. In the case of the RT-type cluster, the centre of the triangular face is occupied by 20 larger atoms such as Mg to form the dodecahedral cluster. The centre of 12 pentagonal faces on the resulting dodecahedron is then filled with smaller atoms Al or X = Zn, Cu, Ag and Pd in the case of the Al–Mg–X system. The second shell formed by these 32 atoms results in the rhombic triacontahedral cluster. The RT-type atom cluster shown in figure 1(a) is, therefore, composed of 44 atoms: 12 atoms in the first shell plus 32 atoms in the second shell.

In the case of the MI-type cluster, 12 atomic sites immediately above 12 atoms on the icosahedron are filled with the TM element such as Fe to form a larger icosahedron. The 30 mid-edge sites on the larger icosahedron are then filled with a mixture of atoms such as Al or Cu atoms. These 54 atoms form the MI-type cluster, as shown in figure 1(b). The atomic structure of the first and second shells in both RT- and MI-type clusters is characterized by $m\bar{3}\bar{5}$ symmetry but a slight distortion is always observed in the 1/1–1/1–1/1 approximants, as described below.

More recently, both a quasicrystal and its 1/1–1/1–1/1 approximant have been discovered in Cd–Yb and Cd–Ca systems (Tsai *et al* 2000, Guo *et al* 2000). The x-ray diffraction spectrum apparently resembles that of the RT-type approximant discussed above. However, it was reported that the Cd-based binary approximant is characterized by a packing of icosahedral clusters having internal symmetry breaking. Further detailed discussion on the Cd-based 1/1–1/1–1/1 approximants seems premature at the present stage.

3. Classification of 1/1–1/1–1/1 approximants

The atomic clusters in figure 1 are located at the body centre and corner of a cubic lattice in the 1/1–1/1–1/1 approximant, as shown in figure 1(c). The two atomic clusters are joined together by glue atoms to form the Wigner–Seitz cell to assure a periodic lattice. Here two cases

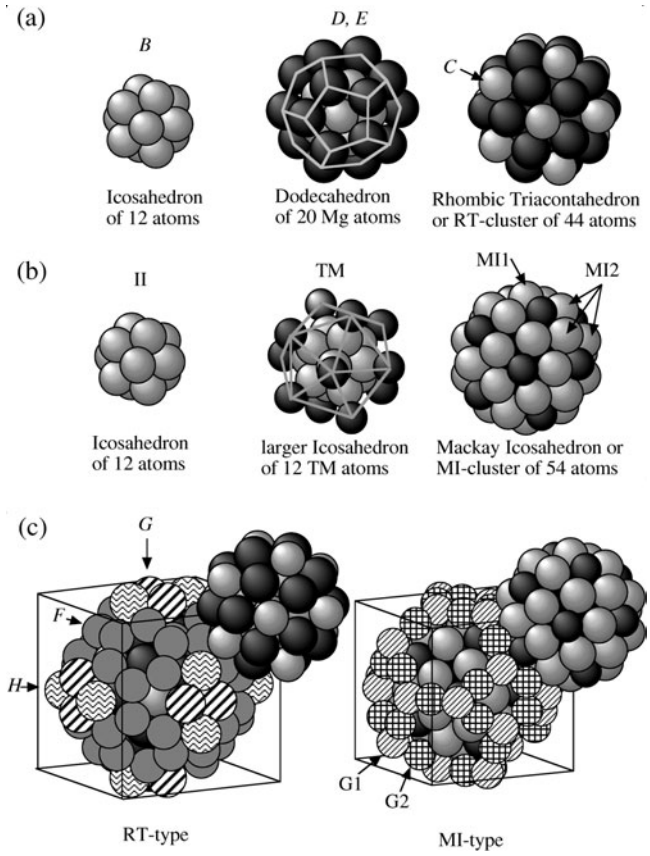

Figure 1. (a) RT- and (b) MI-type atomic clusters and (c) the unit cell of the respective 1/1–1/1–1/1 approximants. Symbols are as follows: A–H in (a) and (c) refer to atomic sites employed by Bergman *et al* (1957). In (b) and (c), II, 12 sites on the first icosahedron; TM, 12 sites on the larger icosahedron; MI1 and MI2, 30 sites on the icosidodecahedron; G1 and G2, glue sites.

exist, depending on whether the two atomic clusters are essentially identical to or different from each other in composition and/or structure. All 1/1–1/1–1/1 approximants, regardless of whether the RT- or MI-type clusters are involved, are now classified into three groups, as listed in table 1.

In order to introduce two different atomic clusters in an icosahedral quasicrystal, two families of lattice nodes, even and odd, are assigned for a simple cubic lattice in six-dimensional space, where the parity refers to that of the sum of the six corresponding coordinates (Boudard *et al* 1992). The superstructure is induced by small differences in atomic hypersurface shapes, volumes and chemical species involved. The situation is essentially the same as for sodium chloride in ordinary three-dimensional space, where its Bravais lattice is a face-centred (F-type) cubic with the basis consisting of one Na atom and one Cl atom separated by one-half the body diagonal of a unit cube of lattice constant $a' = 2a$. This is equivalent to the assignment of two families of lattice nodes mentioned above in a simple cubic lattice.

All indices in reflection lines must be either even or odd, being characteristic of an fcc lattice with the lattice constant a'. However, the structure is essentially reduced to a simple cubic lattice (P type) of lattice constant a, provided that the two atoms happen to possess equal numbers of electrons, like K^+ and Cl^- in KCl. Additional lines exist in NaCl as compared with

Table 1. Classification of 1/1–1/1–1/1 approximants.

Group	Structure type	Space group	Cluster-type	1/1–1/1–1/1 approximants	Structure features
			RT	$Al_xMg_{40}X_{60-x}$ (X =Zn, Cu, Ag and Pd)	
1	P	$Im\bar{3}$	MI	$Al_{68}Cu_7(Fe_{1-x}Ru_x)_{17}Si_8$ $(0 \leqslant x \leqslant 1)$	Two identical clusters at the center and corner of cubic lattice
			MI	$Al_{75}(Mn_{1-x}Fe_x)_{17}Si_8$ $(0.32 \leqslant x \leqslant 0.72)$	
2	P	$Pm\bar{3}$	MI	$Al_{75}(Mn_{1-x}Fe_x)_{17}Si_8$ $(0 \leqslant x \leqslant 0.29)$	Two almost identical clusters at the center and corner of cubic lattice
3	F	$Pm\bar{3}$	MI	$Al_{54}Cu_{25.5}(Fe_{1-x}Ru_x)_{12.5}Si_8$ $(0 \leqslant x \leqslant 1)$	Two different clusters at the center and corner of cubic lattice

KCl. They are assigned as arising from superlattice reflections if the structure is described with the unit cell of lattice constant a. In the case of the six-dimensional Bravais lattice discussed above, only fundamental reflections are observed in the P-type quasicrystals, whereas superlattice reflections are superimposed in the case of the F-type quasicrystals, which signifies the presence of two different atomic clusters arranged quasiperiodically.

We extend the argument above to the generation of the two types of 1/1–1/1–1/1 approximant from the P- and F-type simple cubic lattices in six-dimensional space. The P-type 1/1–1/1–1/1 approximant is generated from the former, where a single lattice node with the lattice constant a is assigned in six-dimensional space. As discussed in the preceding section, it is reduced to either bcc with the space group of $Im\bar{3}$ or simple cubic with the space group of $Pm\bar{3}$. Here the two clusters at the centre and corner of the cubic lattice are essentially the same. On the other hand, the F-type 1/1–1/1–1/1 approximant having two different atomic clusters at the centre and the corner of the cubic lattice with the space group $Pm\bar{3}$ is generated from the latter, where two different lattice nodes with the lattice constant a are assigned in six-dimensional space.

The first group refers to the P-type approximants with the space group of $Im\bar{3}$, in which all the diffraction lines are indexed in terms of the Miller indices characteristic of the bcc structure, i.e. the sum of the Miller indices is always even. The Rietveld refinement is carried out by assuming two identical RT- or MI-type atomic clusters at the body centre and corner of the cubic lattice. Included in this group are the RT-type $Al_{60-x}Mg_{40}X_x$ (X = Zn, Cu, Ag and Pd), the MI-type $Al_{68}Cu_7(Fe_{1-x}Ru_x)_{17}Si_8$ $(0 \leqslant x \leqslant 1)$ and the MI-type $Al_{75}(Mn_{1-x}Fe_x)_{17}Si_8$ $(0.32 \leqslant x \leqslant 0.72)$ 1/1–1/1–1/1 approximants. It is noted that 1/1–1/1–1/1 approximants in this group are always formed near the composition where a thermally stable or metastable P-type quasicrystal is formed.

The second group represents the P-type 1/1–1/1–1/1 approximants with $Pm\bar{3}$ symmetry, where most of the diffraction peaks are indexed in terms of the Miller indices characteristic of the bcc structure but weak diffraction peaks with the Miller indices summed to an odd number remain finite. Though the space group is $Pm\bar{3}$, the two atomic clusters at the centre and corner of the cubic lattice are essentially the same. The typical example in this group is the α-phase Al–Mn–Si 1/1–1/1–1/1 approximant (see section 5.1.1). The Rietveld analysis for other approximants in this group has been performed by using the α-phase Al–Mn–Si approximant

as a starting structure. The atomic structure after the refinement is characterized by two almost identical MI-type atomic clusters at the centre and corner of the cubic lattice. A difference in the degree of chemical disorder in the glue sites is believed to be responsible for reduction of its space group to $Pm\bar{3}$. Included in this group are $Al_{75}(Mn_{1-x}Fe_x)_{17}Si_8 (0 \leqslant x \leqslant 0.32)$ 1/1–1/1–1/1 approximants. The P-type quasicrystals can be formed in the vicinity of the composition of the approximant in this group only as a metastable phase by liquid quenching.

The third group represents the F-type 1/1–1/1–1/1 approximants with the space group of $Pm\bar{3}$ symmetry. Here the two different atom clusters are located at the body centre and the corner of the cubic lattice to form the CsCl-type structure. The approximants in this group are called the F-type and indeed a thermally stable F-type quasicrystal is formed in the vicinity of its composition. As will be shown later, chemical and structural disorder exists both in the glue sites and inside the atom cluster. The degree of disorder in this group is the highest among the three groups. Based on the classification described above, we begin with the determination of the atomic structure followed by the electronic structure calculations and the discussion of the electron transport properties of various 1/1–1/1–1/1 approximants in three different groups.

Unless otherwise stated, the structure of the 1/1–1/1–1/1 approximant was investigated by applying the Rietveld refinement program RIETAN (Izumi 1993) to the powdered diffraction spectrum measured with either a step-scanned laboratory x-ray diffractometer or the beam line 02B2 of the synchrotron radiation facility, SPring-8, Japan.

4. Group 1 (P-type approximants with space group $Im\bar{3}$)

4.1. $Al_xMg_{40}X_{60-x}$(X = Zn, *Cu, Ag and Pd)* 1/1–1/1–1/1 *approximants*

4.1.1. Atomic structure. The atomic structure of the Frank–Kasper compound $(Al, Zn)_{49}Mg_{32}$ was determined by Bergman *et al* (1957) much earlier than the discovery of the quasicrystal (Shechtman *et al* 1984). The complex compound was identified as the bcc structure containing 162 atoms in its unit cell with the lattice constant of 14.16 Å by using a single crystal of 0.1 mm in size with a Weissenberg camera. Following the pioneering work by Shechtman *et al* (1984), Ramachandrarao and Sastry (1985) successfully synthesized the Al–Mg–Zn quasicrystal by making full use of knowledge about the possession of the icosahedral cluster in the Frank–Kasper compound $(Al, Zn)_{49}Mg_{32}$. Indeed, Henley and Elser (1986) pointed out that the Frank–Kasper compound $(Al, Zn)_{49}Mg_{32}$ can be recognized as the 1/1–1/1–1/1 approximant to the icosahedral quasicrystal. Guryan *et al* (1988) determined the atomic structure of the Al–Li–Cu 1/1–1/1–1/1 approximant by applying the Rietveld method to the powdered x-ray and neutron diffraction data.

Takeuchi and Mizutani (1995) obtained a series of the $Al_xMg_{39.5}Zn_{60.5-x}$ single-phase 1/1–1/1–1/1 approximants over the Al concentration range $20.5 \leqslant x \leqslant 50.5$ along the 39.5 at.% Mg concentration line. This was made possible by using the Bergman structure model as a guide, which claims that atomic sites for larger Mg atoms are fixed and remaining sites are shared by a mixture of smaller Al and Zn atoms. Mizutani *et al* (1997) determined the atomic structure of several $Al_xMg_{39.5}Zn_{60.5-x}$ $(20.5 \leqslant x \leqslant 50.5)$ 1/1–1/1–1/1 approximants as a function of the Al concentration. The ingot was melt quenched in order to suppress the grain growth within a few micrometres. Ribbon samples thus obtained were crushed into powders and annealed in a pressurized Ar gas atmosphere for 2 h at 300–450 °C in order to enhance their structural quality. The step-scanned x-ray diffraction spectra were measured with an x-ray diffractometer with a curved pyrolytic graphite single-crystal diffracted beam monochromator with a Cu Kα radiation source. All the diffraction peaks can be indexed in terms of the Miller indices, the sum of which is always even. The Rietveld refinement was,

therefore, accomplished under the condition of the space group $Im\bar{3}$ by using the data due to Bergman *et al* as starting parameters. The structure data were complied as a table in Mizutani *et al* (1997).

The atomic structure is identified as the bcc lattice containing two identical RT clusters shown in figure 1(a) at centre and corner sites plus glue atoms, resulting in 160 atoms in its unit cell. The chemical disordering in the distribution of Al and Zn atoms in both the RT-type atom cluster and the glue sites assures the formation of the bcc structure with the $Im\bar{3}$ symmetry. All Al–Mg–Zn 1/1–1/1–1/1 approximants are classified into the P-type and the P-type quasicrystal is indeed formed near the composition above (Takeuchi and Mizutani 1995). It is shown that the centre of the cluster is only 10% occupied by the Al atom for the sample with $x = 20.5$ and becomes essentially vacant when x exceeds 30. This is the reason why the number of atoms is two atoms less than that reported by Bergman *et al*. Twelve vertex sites of the icosahedral cluster are 80% occupied by Zn atoms and 20% by Al atoms in the concentration range $x \leqslant 40$.

Takeuchi *et al* (2000) reported the atomic structure of other $Al_xMg_{40}X_{60-x}$ 1/1–1/1–1/1 approximants: $Al_xMg_{40}Cu_{60-x}$ ($x = 50$), $Al_xMg_{40}Ag_{60-x}$ ($x = 40$, 42.5, 45, 47.5, 50, 52.5 and 55) and $Al_xMg_{40}Pd_{60-x}$ ($x = 46.5$, 48 and 49.5). The Rietveld analysis was carried out for all these 1/1–1/1–1/1 approximants. To summarize, the atomic structure is universally described by simply replacing the Zn atom by the third element X = Cu, Ag and Pd. In all cases, the centre of the icosahedral cluster is essentially vacant. More specifically, the Al atom always shares atomic sites with the X atom at certain ratios, while the Mg atom occupies its own sites without chemical disorder, as shown in figure 1(a). In the case of the $Al_{5.6}Li_{2.9}Cu$ 1/1–1/1–1/1 approximant, Li is substituted for Mg and Cu for Zn except in site G, where Al is substituted for Mg to maintain its correct stoichiometry (Guryan *et al* 1988).

The total number of valence electrons accommodated in the 12-atom icosahedral cluster is calculated from the refined atomic structure for all approximants studied. The $(e/a)_{ico}$ value defined by dividing the total number of electrons by 12 atoms is plotted in figure 2 as a function of the nominal electron concentration e/a. It is of great interest to note that the $(e/a)_{ico}$ value falls on a universal curve, regardless of the atom species X involved. When the nominal e/a value is <2.3, the electron concentration $(e/a)_{ico}$ in the icosahedral cluster is always lower than the nominal one and is close to the value of 2.15. This is the electron concentration at which a thermally stable quasicrystal is formed in the systems with X = Zn and Pd (Takeuchi *et al* 1994, Takeuchi and Mizutani 1995, Koshikawa *et al* 1993). The e/a value of 2.15 is indeed the electron concentration at which the Hume–Rothery matching rule is satisfied for the Al–Mg–Zn quasicrystal (Takeuchi and Mizutani 1995). Hence, the possession of an average electron concentration of 2.15 on the icosahedral cluster should be of critical importance to stabilize a system containing the icosahedral cluster. However, the value of $(e/a)_{ico}$ begins to increase rapidly when the nominal electron concentration exceeds 2.3. This suggests that the electronic effect becomes less important and is most likely superseded by the size effect in the e/a range above 2.3. The importance of the size effect is hinted at by the fact that the 1/1–1/1–1/1 approximant is always formed along the 39.5–40.0 at.% Mg concentration line and smaller Al and X atoms are apparently filling the space formed by the network of larger Mg atoms in a compacted manner.

Finally, we discuss the symmetry of the icosahedral cluster in the Al–Mg–X 1/1–1/1–1/1 approximants. Though all edge lengths of a perfect icosahedron are equal to each other and the symmetry of $m\bar{3}\bar{5}$ holds, the icosahedral cluster found in the 1/1–1/1–1/1 approximant discussed above is generally distorted: two different edge lengths are observed and, thus, the symmetry is reduced to $m\bar{3}$. Figure 3 shows the ratio of the shorter edge length over the longer one for all RT-type 1/1–1/1–1/1 approximants studied. Recall that about 80% of 12

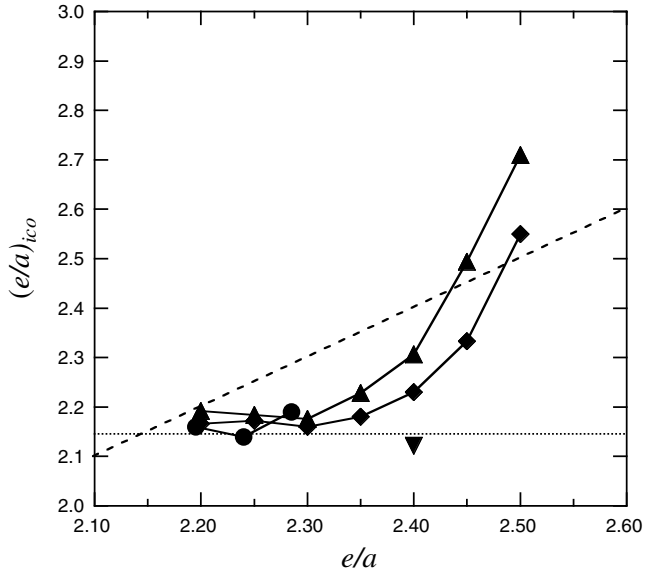

Figure 2. e/a, i.e. $(e/a)_{nominal}$, dependence of $(e/a)_{ico}$ in the first icosahedral cluster in the various RT-type 1/1–1/1–1/1 approximants (Takeuchi *et al* 2000). The dotted line with $(e/a)_{ico} = 2.15$ refers to the overall electron concentration where the quasicrystals are stabilized. The dashed line denotes the line $(e/a)_{ico} = (e/a)_{nominal}$. ♦: Al–Mg–Zn, ▼: Al–Mg–Cu, ▲: Al–Mg–Ag and ●: Al–Mg–Pd.

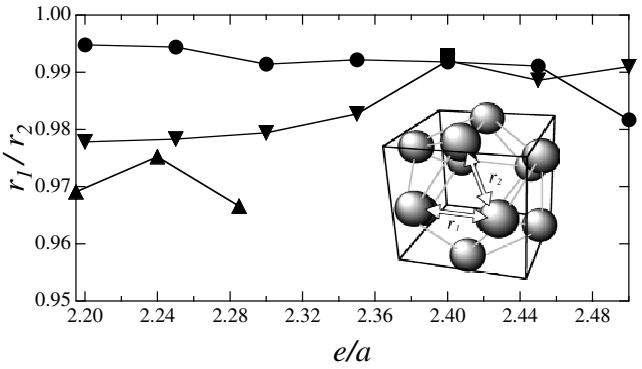

Figure 3. e/a dependence of the ratio of the shorter edge length over the longer one in the first icosahedral cluster of various RT-type 1/1–1/1–1/1 approximants (Takeuchi *et al* 2000). ●: Al–Mg–Zn, ■: Al–Mg–Cu, ▼: Al–Mg–Ag and ▲: Al–Mg–Pd.

atomic sites on the icosahedron is occupied by X atoms whereas the remaining 20% by Al atoms. Thus, the distortion is most likely introduced as a result of the difference in the degree of hybridization between the 3p states of the Al atom and the d states of the X atom on the icosahedral cluster, since the degree of distortion apparently increases in the order of Zn, Cu, Ag, Pd, or increasing d states near the Fermi level. Indeed, the hybridization effect was clearly observed in the spectra of photoemission and soft-x-ray spectroscopies and its effect increases when the third element X moves from Zn, Cu, Ag to Pd (Mizuno *et al* 1999). From this it was concluded that the stronger the hybridization is, the more the icosahedral cluster in the 1/1–1/1–1/1 approximant is distorted.

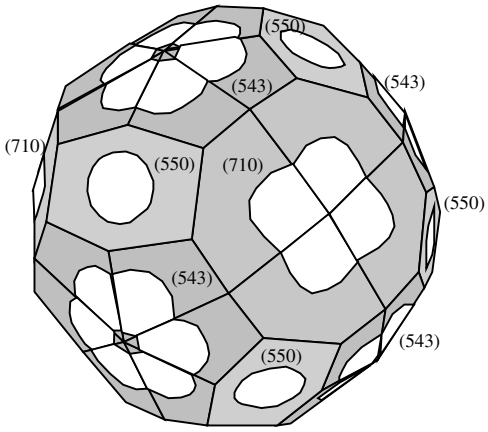

Figure 4. The Brillouin zone of 24-fold {710}, 48-fold {543} and 12-fold {550} planes with the free-electron Fermi sphere for the $Al_{30}Mg_{40}Zn_{30}$ 1/1–1/1–1/1 approximant (Sato *et al* 2001).

4.1.2. Electronic structure. The Fermi diameter $2k_F$ in the free-electron model is found to coincide with the magnitude of the reciprocal lattice vector corresponding to 48-fold {543}, 24-fold {710} and 12-fold {550} zone planes in the middle of the composition range of $Al_xMg_{39.5}Zn_{60.5-x}$ ($20.5 \leqslant x \leqslant 50.5$) 1/1–1/1–1/1 approximants (Takeuchi and Mizutani 1995). Note that 84 zone planes are at the same distance from the origin. The Brillouin zone consisting of these 84 zone planes along with the free-electron sphere with the electron concentration $e/a = 2.3$ is illustrated in figure 4. Regarding the band calculations, Hafner and Krajcí (1993) were the first to reveal the pseudogap at the Fermi level in the $Al_{16}Mg_{40}Zn_{44}$ 1/1–1/1–1/1 approximant, the atomic structure of which was generated theoretically by the projection method. Unfortunately, however, the composition they chose falls outside the region where the 1/1–1/1–1/1 approximant exists as a single phase. In connection with the Hume–Rothery rule, they noted without any proof, like showing dispersion relations across the centre of zones that the pseudogap at the Fermi level is induced by the zone effects associated with closely spaced {631}, {710} + {550} and {640} planes.

The valence band structure for the $Al_{30}Mg_{40}Zn_{30}$ 1/1–1/1–1/1 approximant was more recently calculated by using the experimentally derived atomic structure, as discussed in the preceding section, while ignoring chemical disorder (Sato *et al* 2001). Figure 5(a) shows the energy dispersion relation along the ⟨710⟩ direction in comparison with the corresponding free-electron one in (b). Clearly, the electronic structure of this particular approximant can be well described by the nearly-free-electron model except for the presence of the Zn 3d states near the bottom of its valence band. The pseudogap, though it is shallow, is clearly found across the Fermi level, as shown in figure 5(c).

Sato *et al* noted that highly degenerate free-electron states at the centre of {543}, {710} and {550} planes in the extended zone scheme are all reduced to the region at the point N corresponding to the centre of the {110} zone planes in the reduced zone scheme and proved that the lifting of these degenerate states leads to the pseudogap at the Fermi level. It is concluded that the electronic structure of the $Al_{30}Mg_{40}Zn_{30}$ 1/1–1/1–1/1 approximant is best approximated by the nearly-free-electron model and thereby the Fermi surface–Brillouin zone interaction is solely responsible for the formation of a rather shallow pseudogap at the Fermi level.

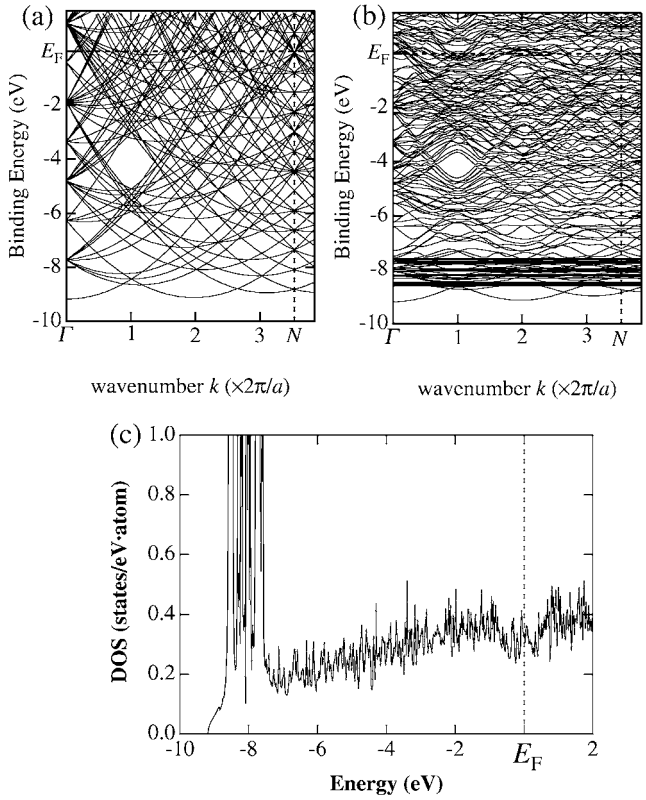

Figure 5. Dispersion relations along the ⟨710⟩ direction in (a) the free electron model, (b) the LMTO–ASA band calculations and (c) the density of states for the $Al_{30}Mg_{40}Zn_{30}$ 1/1–1/1–1/1 approximant (Sato *et al* 2001). The vertical line in (a) and (b) corresponds to the centre N of the {710} zone planes.

4.1.3. Electron transport properties. The validity of the nearly-free-electron model, a shallow pseudogap at the Fermi level and only a small perturbation due to the hybridization effect should lead to relatively low electrical resistivities in the family of the Al–Mg–X 1/1–1/1–1/1 approximants. Indeed, the electrical resistivity at room temperature is distributed over 40–200 $\mu\Omega$ cm: 40–70 $\mu\Omega$ cm for X = Zn, 80–140 $\mu\Omega$ cm for X = Ag and 120–210 $\mu\Omega$ cm for X = Pd (Mizuno *et al* 1999). Though the magnitude of resistivities is much lower than those in other approximants discussed below, we clearly notice an increase in resistivity in the order of X = Zn, Ag, Pd. The XPS and soft-x-ray spectroscopy measurements revealed the shift of the d states towards the Fermi level in this sequence (Mizuno *et al* 1999). Thus, this behaviour is well interpreted as the reflection of an increasing degree of hybridization between the 3p states of Al and d states of the element X. The nearly-free-electron-like electronic structure is valid only for X = Zn and the hybridization effect gradually increases with decreasing electron per atom ratio of the element X. Takeuchi *et al* (2001) could consistently interpret the scattering mechanism in all Al–Mg–X 1/1–1/1–1/1 approximants in terms of the degrees of chemical disorder and of the sp–d hybridization within the context of the Boltzmann transport equation. Thus, we say that the chemical species dependence of resistivity clearly reflects the electronic structure in the short-range atomic cluster.

What about the effect due to the long-range order? It is of great interest at this stage to compare the resistivity values at 300 K of various RT-type Al–Mg–X 1/1–1/1–1/1 approximants with those of the corresponding quasicrystals. The resistivity of 150 $\mu\Omega$ cm for the Al–Mg–Zn quasicrystal is almost three times as large as that of its approximant (Takeuchi and Mizutani 1995). The electron mean free path estimated from the resistivity value

turned out to decrease from 15 to 20 Å in the approximant down to about 5–10 Å in the quasicrystal (Mizutani 2000). This clearly implies that the destruction of the periodic potential in the quasicrystal results in a decrease of the mean free path and a sharp increase in the resistivity and thereby is taken as a clear demonstration for the long-range order effect. However, the situation changes when the resistivity becomes higher. The resistivity value of the Al–Mg–Pd quasicrystal is only slightly higher than that of the corresponding 1/1–1/1–1/1 approximant, both being in the neighbourhood of 200–210 $\mu\Omega$ cm at 300 K (Hashimoto *et al* 1994). Note here that the electron mean free path is already comparable to an average atomic distance in both quasicrystal and approximant. Thus, the mean free path effect is no longer effective and, instead, the resistivity value is decided by the electronic structure at the Fermi level (Mizutani 2000).

4.2. $Al_{68}Cu_7(Fe_{1-x}Ru_x)_{17}Si_8 (0 \leqslant x \leqslant 1)$ 1/1–1/1–1/1 approximant

4.2.1. Atomic structure. In previous sections, we have discussed the P-type approximant composed of the RT-type atomic clusters with $Im\bar{3}$ symmetry. In contrast, the approximants in this section are built up from the MI-type clusters shown in figure 1(b), which are located at the body centre and corner of a cubic lattice to form the bcc structure. They are classified into the P type, since only the fundamental reflection lines are observed. Indeed, metastable P-type quasicrystals can be formed by liquid quenching in the vicinity of the composition of the $Al_{68}Cu_7(Fe_{1-x}Ru_x)_{17}Si_8$ ($0 \leqslant x \leqslant 1$) 1/1–1/1–1/1 approximants.

The atomic structure of the $Al_{68}Cu_7(Fe_{1-x}Ru_x)_{17}Si_8$ ($x = 0$, 0.5 and 1) 1/1–1/1–1/1 approximants is determined by analysing the powdered diffraction spectra taken with the SPring-8 beamline 02B2 in the synchrotron radiation facility, Japan, by means of the Rietveld method and the resulting structure data are reported (Mizutani *et al* 2001, Takeuchi and Mizutani (2001)). The space group is reduced to $Im\bar{3}$ as a result of averaging of chemical disorder in the glue sites over a whole crystal. Chemical disorder in the distribution of Al and Cu atoms also exists in the first and second shells of the MI-type cluster. The TM element Fe or Ru is exclusively located at 12 vertices of the larger icosahedron. However, these 12 sites are shared randomly by Fe and Ru atoms in proportion to the composition ratio x, when x is in the range $0 < x < 1$. The remaining 30 mid-edge sites on the larger icosahedron are occupied with a mixture of about 90% Al and 10% Cu atoms.

4.2.2. Electronic structure. The LMTO–ASA band calculations have been performed for the $Al_{68}Cu_7Ru_{17}Si_8$ 1/1–1/1–1/1 approximant after a slight modification of the experimentally determined atomic structure: the presence of Cu atoms with occupancies of 4–13% with remaining Al atoms on the sites II, MI1, MI2 and G3 is completely ignored and all these sites are replaced by Al atoms whereas Cu and Si atoms are located only on the glue sites G1 and G2 (Mizutani *et al* 2001).

As shown in figure 6(a), a deep pseudogap is found across the Fermi level and its origin is interpreted as the superposition of the Fermi surface–Brillouin zone interaction satisfying the Hume–Rothery matching rule and the sp–d hybridization effect (Mizutani *et al* 2001). The sp–d hybridization terms in wavefunctions, where sp states refer to the Al 3s, Al 3p, Si 3s and Si 3p states whereas d states Cu 3d and/or Ru 4d states, are intentionally deleted to suppress the sp–d hybridization effect. The resulting sp partial DOS is shown in figure 6(b). Obviously, the pseudogap remains finite above the Fermi level, though its magnitude is substantially reduced and becomes comparable to that in the Al–Mg–Zn approximant in figure 5(c). This clearly indicates that the sp–d hybridization effect characterizing the bonding nature in the atomic cluster substantially contributes to deepening the pseudogap at the Fermi level in favour of the

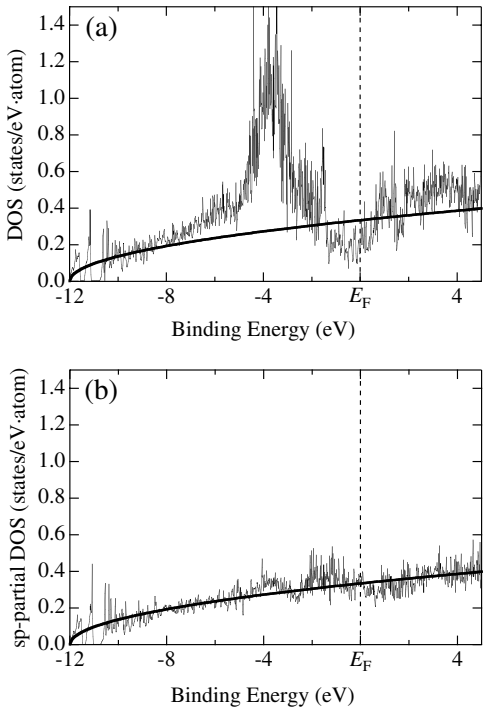

Figure 6. (a) Total density of states and (b) sp partial density of states for the $Al_{68}Cu_7Ru_{17}Si_8$ 1/1–1/1–1/1 approximant (Mizutani *et al* 2001).

stabilization of the compound, but that the effect of the long-range order cannot be neglected and should be also properly taken into account.

4.2.3. Electron transport properties. The temperature dependence of the electrical resistivity for the P-type $Al_{68}Cu_7(Fe_{1-x}Ru_x)_{17}Si_8$ ($x = 0, 0.5$ and 1) 1/1–1/1–1/1 approximants is shown in figure 7. All of them exhibit a positive temperature coefficient of resistivity (TCR) over a whole temperature range 2–300 K with residual resistivities 520–730 $\mu\Omega$ cm (Takeuchi and Mizutani 2001). This is consistent with the scattering mechanism based on the Boltzmann transport equation in spite of the possession of large resistivities exceeding 500 $\mu\Omega$ cm. This is possible in a system where the density of states at the Fermi level is fairly low but the chemical disordering is weak enough to assure the mean free path of electrons longer than an average atomic distance of several ångstroms (Mizutani 2000).

Note that the resistivity is certainly much higher than those found in the Al–Mg–X approximants involving the RT-type clusters. Figure 8(a) shows the three-dimensional atom distributions in the first and second shells of the atomic cluster in the $Al_{68}Cu_7Ru_{17}Si_8$ 1/1–1/1–1/1 approximant. The charge distribution of electrons at the Fermi level in the (200) plane is shown in figure 8(b) (Mizutani *et al* 2001). A region where the electron density is high or low is shown with a brighter or darker contrast, respectively. We see that the directional charge distribution reminiscent of the covalent bonding is indeed significant between the Ru and Al atoms, and that regions where the charge distribution is high are essentially limited to those connecting Ru and Al atoms. This means that electrons at the Fermi level can flow exclusively along channels connecting the Ru 4d and Al 3p states. Such a small channel coupled with strongly localized tendency of 4d electrons must be responsible for the possession of a high resistivity in the $Al_{68}Cu_7Ru_{17}Si_8$ 1/1–1/1–1/1 approximant in sharp contrast to the nearly-free-electron-like Al–Mg–Zn approximant. The analysis above certainly points to the

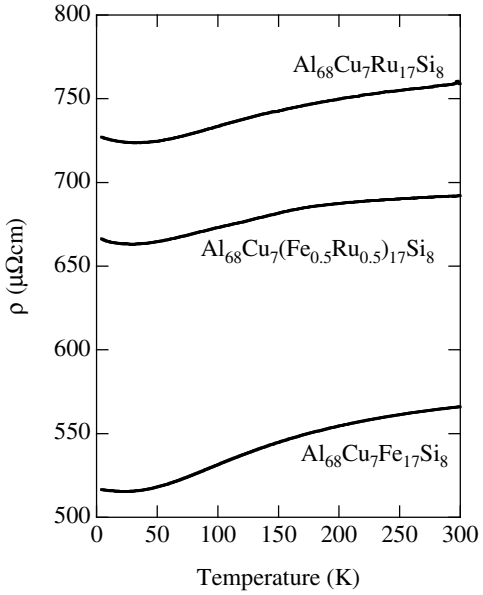

Figure 7. Temperature dependence of electrical resistivity for the P-type $Al_{68}Cu_7(Fe_{1-x}Ru_x)_{17}Si_8$ ($x = 0$, 0.5 and 1) 1/1–1/1–1/1 approximants (Takeuchi and Mizutani 2001).

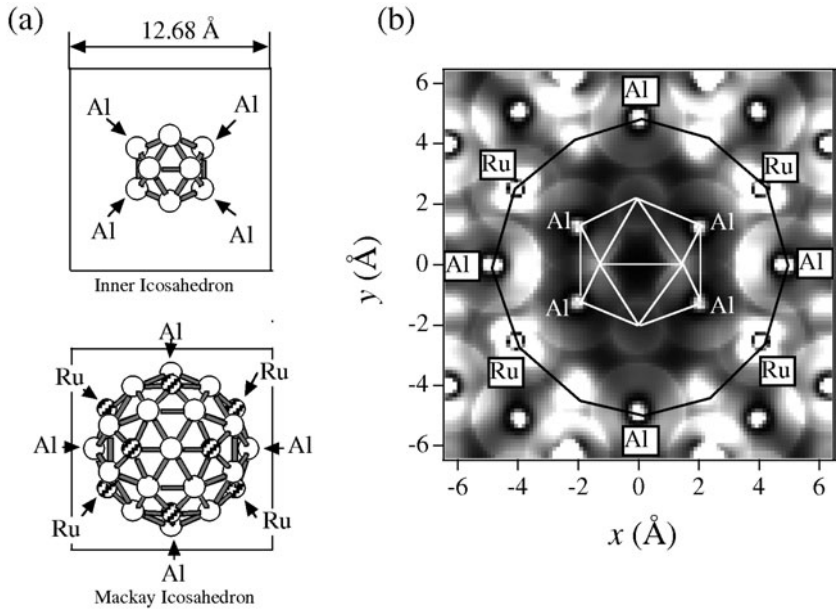

Figure 8. (a) Atom distributions in the first and second shells of the MI cluster in the $Al_{68}Cu_7Ru_{17}Si_8$ 1/1–1/1–1/1 approximant and (b) charge distribution of electrons at the Fermi level in the (200) plane of this approximant (Mizutani *et al* 2001).

importance of the effect of the short-range bonding character in the atomic cluster on the electron transport properties.

We can draw a further conclusion from figure 8(b). The charge distribution in the first icosahedral cluster is substantially dark and thus deficient. This means that electrons in the vicinity of the icosahedral cluster are pushed into higher binding energies, thereby lowering the electronic energy in this system. Therefore, the icosahedral cluster is found to play a critical role in stabilization of such a complex electron compound. The situation is believed to be the same in the corresponding quasicrystal. The stabilization mechanism discussed above is simply based on the charge distribution of the atomic cluster in real space. We are well aware that the Fermi surface–Brillouin zone interaction, which reflects the long-range order, is also carefully taken into account; otherwise the existence of different stable composition ranges for a quasicrystal and the corresponding approximant cannot be properly understood.

4.3. $Al_{75}(Mn_{1-x}Fe_x)_{17}Si_8$ ($0.32 \leqslant x \leqslant 0.72$) 1/1–1/1–1/1 approximants

4.3.1. Atomic structure. First of all, we discuss the formation range of the Al–(Mn, Fe)–Si 1/1–1/1–1/1 approximants. The approximant free from a second phase can be formed, provided that Si concentration is fixed at 8–9 at.% in the chemical formula $(Al, Si)_{82}Mn_xFe_{18-x}$ (Takeuchi *et al* 2001). The Al primary phase immediately precipitated when the composition departs from the composition line $(Al, Si)_{82}Mn_xFe_{18-x}$ toward the (Al, Si)-rich side. Instead, Al_9Mn_3Si and unknown phase(s) appeared on the other side of this line. As will be discussed below, a slight structure modification has to be introduced into the 1/1–1/1–1/1 approximant in stabilizing the 1/1–1/1–1/1 phase upon the replacement of Mn by Fe atoms.

For the sake of simplicity, the chemical formula $Al_{75}(Mn_{1-x}Fe_x)_{17}Si_8$ is employed instead of $(Al, Si)_{82}Mn_xFe_{18-x}$ above. Takeuchi *et al* (2001) studied a change in the atomic structure as a function of x over the range $0 \leqslant x \leqslant 0.69$. The diffraction spectra are shown in figure 9(a) and the Bragg peaks in the angle range $35° < 2\theta < 42°$ are blown up in figure 9(b). Note that intensities of the diffraction lines having Miller indices whose sum is equal to an odd number, such as (500), (511), (520) and (533), are weak but finite, as long as the Fe concentration x is below 0.29. However, these diffraction lines disappear in the range $x \geqslant 0.32$ (see data (D)–(G)). This clearly implies that the simple cubic lattice transforms to the bcc lattice above the Fe concentration $x = 0.32$. Indeed, the atomic structure of the Al–Mn–Si 1/1–1/1–1/1 approximant free from Fe, i.e. $x = 0$, is known to consist of two almost identical Mackay icosahedral clusters at body-centred and vertex sites of the cubic lattice, and atoms at glue sites connecting the two Mackay clusters break the symmetry of the bcc structure, resulting in a simple cubic lattice with the space group of $Pm\bar{3}$ (Cooper and Robinson1966, Sugiyama *et al* 1998a).

The 1/1–1/1–1/1 approximants in the range $0.32 \leqslant x \leqslant 0.69$ are then classified into the first group as being typical of the P type with the space group of $Im\bar{3}$ (Takeuchi and Mizutani 2001). The Rietveld analysis was made by using the diffraction data taken for the $Al_{73.5}Mn_{11.3}Fe_{6.2}Si_9$ approximant, which is denoted as (E) in figure 9. All reliability factors (R-factors) are reduced to below 2% and the composition deduced from the refined structure is well consistent with the nominal one. The structure data are listed in Takeuchi *et al* (2001). One can see from the Rietveld analysis that sites II, MI1 and MI2 in the MI-type cluster are exclusively occupied by Al atoms and that sites TM are filled only with the TM elements Mn and Fe. The occupancy of the Fe atoms over the TM sites is found to be 0.37 for the 6.2 at.% Fe sample or $x = 0.36$. This indicates that Mn and Fe atoms are randomly distributed only over the TM sites.

It is suggested that Si atoms would fill only the glue sites, the number of which requires the Si concentration of 8.3 at.% (Mizutani *et al* 2001). This implies that the addition of 8–9 at.% Si is critically important in stabilizing the 1/1–1/1–1/1 approximant in place of the quasicrystalline counterpart. Indeed, the Si concentration was fixed at 8–9 at.% in the

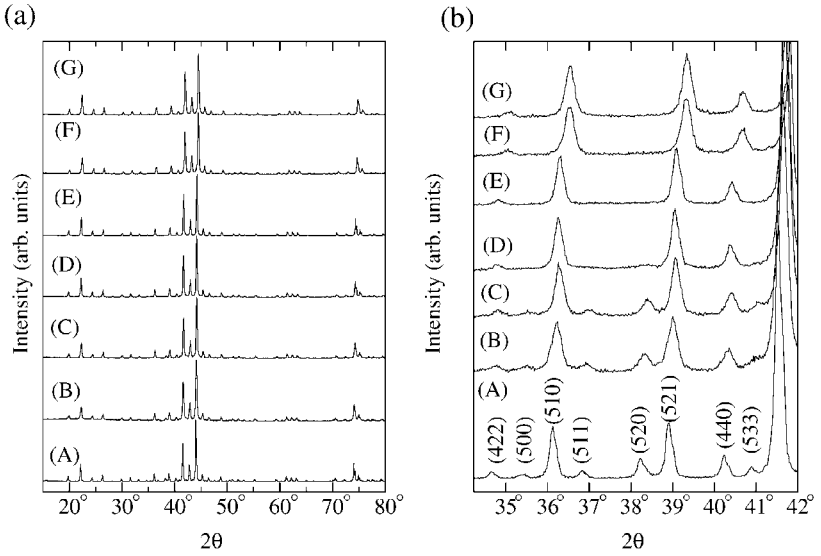

Figure 9. (a) XRD spectra for a series of Al–Mn–Fe–Si 1/1-cubic approximants, (A) $Al_{73.6}Mn_{17.4}Si_9$, (B) $Al_{73.6}Mn_{14.9}Fe_{2.5}Si_9$, (C) $Al_{73.6}Mn_{12.4}Fe_{5.0}Si_9$, (D) $Al_{73.5}Mn_{11.9}Fe_{5.6}Si_9$, (E) $Al_{73.5}Mn_{11.3}Fe_{6.2}Si_9$, (F) $Al_{73}Mn_8Fe_{10}Si_9$ and (G) $Al_{73}Mn_{5.5}Fe_{12.5}Si_9$. (b) XRD spectra in the range $34° \leqslant \theta \leqslant 42°$. Diffraction lines whose Miller indices are summed to an odd number are less intense than others. These peaks disappear in samples (D)–(G), indicating the phase transformation from a simple cubic to bcc structure (Takeuchi *et al* 2001).

measurement described above. However, different Si concentrations such as 12 at.% had been employed for the Al–Mn–Si 1/1–1/1–1/1 approximant in the literature (Sugiyama *et al* 1998, Kirihara *et al* 2000). Further work is needed to determine the Si solid solution range. For this particular purpose, a combination of the x-ray and neutron diffraction measurements is of great help to distinguish Si from Al.

More interesting is the fact that the occupancy of atoms in the glue sites decreases significantly with increasing Fe concentration beyond $x = 0.32$, despite the fact that the Mackay clusters remain essentially unchanged. This leads to a decrease in the total number of atoms in the unit cell. Takeuchi *et al* (2001) proposed that the number of vacancies increases so as to fulfill the Hume–Rothery matching rule by adjusting the electron concentration per unit cell and took this adjustment as the stabilization mechanism of the Fe-bearing $Al_{75}(Mn_{1-x}Fe_x)_{17}Si_8$ 1/1–1/1–1/1 approximants.

5. Group 2 (P-type approximants with space group $Pm\bar{3}$)

5.1. $Al_{75}(Mn_{1-x}Fe_x)_{17}Si_8 (0 \leqslant x \leqslant 0.29)$ 1/1–1/1–1/1 approximants

5.1.1. Atomic structure. As discussed in section 4.3.1, the approximant with $x = 0$ corresponds to the well known α-phase Al–Mn–Si compound (Cooper and Robinson 1966), which was identified as the 1/1–1/1–1/1 approximant to the P-type Al–Mn quasicrystal by Elser and Henley (1985). The atomic structure of the Al–Mn–Si 1/1–1/1–1/1 approximant has been studied more recently by Sugiyama *et al* (1998) and Kirihara *et al* (2000). Both groups consistently concluded that 12 sites of the first icosahedron (see figure 1(b)) are filled by a mixture of Al and Si atoms, while 12 sites of a larger icosahedron and 30 sites of the icosidodecahedron, the latter of which forms the atomic cluster of the so-called

icosidodecahedron, are exclusively occupied by Mn and Al atoms, respectively. The two atomic clusters thus obtained are located at the centre and vertex of a cubic lattice and are connected with each other by glue atoms with the space group $Pm\bar{3}$.

The P-type 1/1–1/1–1/1 approximant with the space group of $Pm\bar{3}$ can be retained up to $x \leqslant 0.29$ in $Al_{75}(Mn_{1-x}Fe_x)_{17}Si_8$. The structure data deduced from the Rietveld analysis for the samples $Al_{73.6}Mn_{17.4}Si_9$ and $Al_{73.6}Mn_{12.4}Fe_{5.0}Si_9$ are listed in Takeuchi *et al* (2001). All reliability factors (R-factors) are reduced to below 5% and the composition deduced from the refined structure is well consistent with the nominal one. In contrast to the data for the $Al_{73.5}Mn_{11.3}Fe_{6.2}Si_9$ with the $Im\bar{3}$ symmetry, sites II, MI, TM and G in this group are further divided into subgroups a and b. It was noted that sites IIa and IIb in the first icosahedral cluster and sites MI1a, MI1b, MI2a and MI2b in the icosidodecahedral cluster are again exclusively occupied by Al atoms, and that the TMa and TMb sites in the larger icosahedral cluster are filled only with the TM elements Mn and/or Fe. The occupancy of the Fe atoms in the sites TMa and TMb is found to be 0.2 and 0.4 for the sample with $x = 0.29$, respectively.

It is also of great interest to discuss what is the most probable stoichiometric composition for the Al–Mn–Si 1/1–1/1–1/1 approximant. Judging from the data for sample (A) with 9 at.% Si, all the sites except for glue sites G and sites TM are occupied only by Al atoms without any chemical disorder. The glue sites G are a little more complicated. The sites G1 are shared by Si and Al atoms in the proportion 1:4. The sites G2a are filled with Al atoms with 4% vacancies, whereas G2b with Si atoms with 11% vacancies. From the data above we see that 138 atomic sites in the unit cell are occupied by the three constituent atoms in the ratio Al:Mn:Si = 102:24:12, which leads to the chemical formula of $Al_{17}Mn_4Si_2$. We believe that the composition $Al_{73.6}Mn_{17.4}Si_9$ or $Al_{17}Mn_4Si_2$ is the stoichiometric composition for the Al–Mn–Si approximant having only Al atoms in the first icosahedral shell.

5.1.2. Electronic structure. The first theoretical demonstration of the existence of the pseudogap at the Fermi level in the 1/1–1/1–1/1 approximant was made by Fujiwara (1989) by using the idealized α-phase Al–Mn approximant containing 114 Al atoms and 24 Mn atoms while ignoring Si atoms. Its depth is fairly deep and comparable to that in figure 6 for the Al–Cu–Ru–Si approximant, indicating that the sp–d hybridization between the Al 3p and Mn d states plays a key role in the formation of a deep pseudogap at the Fermi level. Indeed, the formation of the covalent bonding between Al and Mn atoms can be clearly seen in the electron-density maps for the Al–Mn–Si 1/1–1/1–1/1 approximant (Kirihara *et al* 2000).

5.1.3. Electron transport properties. Tamura *et al* (2001) revealed that their newly synthesized $Al_{72.5}Re_{17.4}Si_{10.1}$ 1/1–1/1–1/1 approximant is isostructural to the the α-phase Al–Mn–Si compound characterized by the P type and the space group $Pm\bar{3}$ and reported its electrical resistivity behaviour measured over the temperature range 12–300 K. Its resistivity value after annealing is found to be very high and reaches 10 000 $\mu\Omega$ cm. A pronounced negative TCR was observed over the whole temperature range and the ratio $\rho_{12\ K}/\rho_{300\ K}$ exceeded two. They considered this behaviour to be reminiscent of the weak localization effect and generic to the geometry of the atomic structure, similar to those found in the icosahedral phase.

6. Group 3 (F-type approximants with space group $Pm\bar{3}$)

6.1. Al–Cu–Fe–Si 1/1–1/1–1/1 *approximants*

6.1.1. Atomic structure. A thermally stable $Al_{62}Cu_{25.5}Fe_{12.5}$ quasicrystal was discovered by Tsai *et al* (1987) and its identification as the F type was discussed by Devaud-Rzepski

et al (1989). Quivy *et al* (1996) reported the formation of the Al–Cu–Fe–Si 1/1–1/1–1/1 approximant by substituting Si for Al in the Al–Cu–Fe icosahedral quasicrystal. The Al–Cu–Fe–Si 1/1–1/1–1/1 approximant is formed near the F-type quasicrystal and is proved to be typical of the F-type approximant involving two different atomic clusters in its unit cell, as will be described below.

The formation range and the atomic structure of the F-type Al–Cu–Fe–Si 1/1–1/1–1/1 approximant were studied by Yamada *et al* (1998) by combining powdered x-ray Rietveld analysis and high-angle annular dark-field scanning transmission electron microscopy (HAADF-STEM). Two series of alloys, $Al_{55}Si_7Cu_{38-x}Fe_x$ ($x = 7.5$, 10, 12.5, 15 and 17.5) and $Al_{62-y}Si_yCu_{25.5}Fe_{12.5}$ ($y = 1$, 3, 5, 7, 8, 9, 10, 11 and 13), were selected to determine the formation range of both the quasicrystal and the approximant. Ribbon samples produced by the melt spinning method were annealed at temperatures below the melting point to improve the structural quality of both quasicrystal and approximant. A quasicrystalline single phase was formed in the range $0 \leqslant y \leqslant 3$, whereas the 1/1–1/1–1/1 approximant of the highest quality was free from a second phase only in a narrow composition range centred at $Al_{53}Si_9Cu_{25.5}Fe_{12.5}$, which differs by 2% in Al and Si contents from the composition of $Al_{55}Si_7Cu_{25.5}Fe_{12.5}$ reported by Quivy *et al* (1996).

Electron diffraction patterns taken along the [100], [110] and [111] directions are consistent with the possession of a simple cubic lattice and are characteristic of symmetries of $2mm$, $2mm$ and 6, respectively. Thus, the space group of the $Al_{53}Si_9Cu_{25.5}Fe_{12.5}$ 1/1–1/1–1/1 approximant is proved to be $Pm\bar{3}$. The Rietveld analysis was performed by employing the structure of the α-phase Al–Mn–Si as a starting structure. The final structure parameters obtained after the refinement are listed in the literature (Yamada *et al* 1998). The lattice constant is deduced to be 12.319 Å. The second shell including 12 sites of the larger icosahedron and 30 sites of the icosidodecahedron in one of the sublattices is dominated by the late transition element Cu, while that in the other sublattice is nearly the same as that in the α-phase Al–Mn–Si in the sense that 30 icosidodecahedral sites are occupied only by Al atoms. This clearly indicates the formation of the CsCl-type structure, thereby being designated as the F-type.

The HAADF-STEM measurement was carried out to determine the position of heavy atoms, since the contribution of each constituent element to the image is proportional to the square of their atomic numbers (Z^2-contrast). The HAADF-STEM images taken along [100], [110] and [111] directions are reproduced from Takeuchi *et al* (2000) in figure 10(a) together with the calculated images (b) from the Rietveld-refined structure. A bright portion of both the observed and calculated images corresponds to the projected position of the TM atoms Cu and/or Fe on a plane perpendicular to the direction of an incident electron beam. The dark area, on the other hand, corresponds to that of lighter elements Al and/or Si or vacancies. In the images of the [100] direction, we can directly confirm that two different clusters exist and form the CsCl-type cubic structure. Indeed, more TMs are found in one cluster than in the other, in good agreement with images calculated from the atomic structure deduced from the Rietveld analysis. This is a straightforward demonstration for the formation of the F-type 1/1–1/1–1/1 approximant in this system.

In the course of the structural refinement, Takeuchi *et al* (2000) revealed that the thermal parameter B_{iso} of the atoms on the inner icosahedral shell II in the sublattice, in which the concentration of the TM is high, is exceptionally large, sometimes exceeding 10 Å^2, and its occupancy is lowered to 70–80%. This led them to presume the existence of a distortion of the inner icosahedral shell and to introduce a single vacancy into shell II with subsequent structural relaxation. The single vacancy thus introduced should be located with an equal probability over 12 equivalent sites to preserve the overall space symmetry $Pm\bar{3}$. The new atomic configurations II$'$ and II$''$ were obtained, as described in the literature (Takeuchi *et al* 2000) . Both the

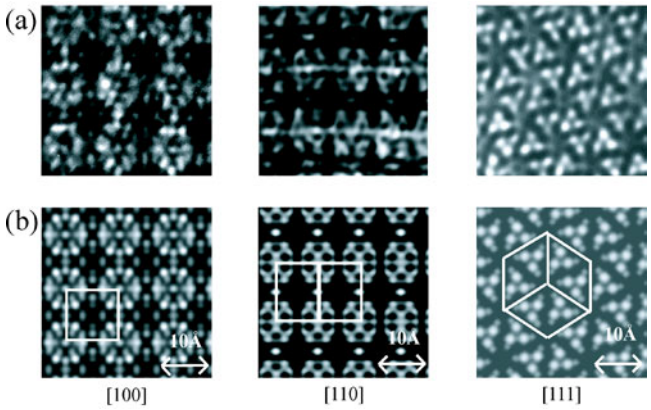

Figure 10. (a) HAADF-STEM images taken along [100], [110] and [111] directions and (b) the projection of the atomic structure deduced from the Rietveld refinement. A white line indicates the edge of a cubic unit cell (Takeuchi *et al* 2000).

(This figure is in colour only in the electronic version)

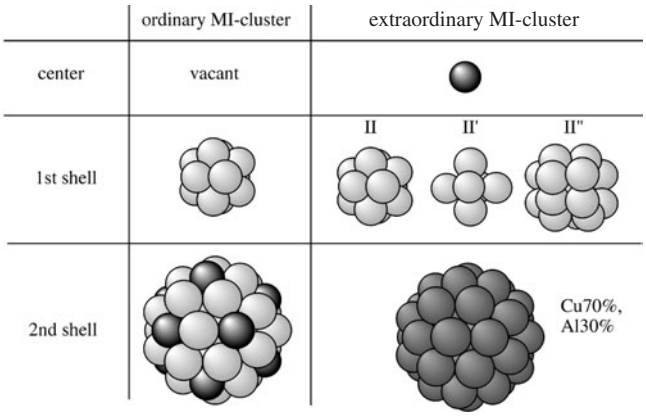

Figure 11. Two atomic clusters in the F-type 1/1–1/1–1/1 approximants. The centre is vacant in the ordinary MI cluster but is filled with Cu in the extraordinary one. The first shell in the latter has three possible atomic configurations due to an introduction of a single vacancy into 12 equivalent sites. The second shell in the former consists of 12 TM atoms on the larger icosahedron and 30 Al atoms on the icosidodecahedron, whereas these 42 atomic sites are randomly shared by 70% of Cu and 30% of Al in the latter.

reliability factor R and thermal parameter B_{iso} in the Rietveld analysis were successfully reduced to a satisfactory level by assuming the new atomic configurations II′ and II″ along with the original one II.

From the discussion above they concluded that the F-type Al–Cu–Fe–Si 1/1–1/1–1/1 approximant stabilizes only at a very specific composition in the neighbourhood of $Al_{53}Cu_{25.5}Fe_{12.5}Si_9$ with the space group of $Pm\bar{3}$ and is characterized by the CsCl-type cubic structure with one sublattice containing more TMs and the other fewer TMs. They are called the ordinary and extraordinary MI-type clusters, as illustrated in figure 11. The presence of the 'structural disorder' in the first shell of the extraordinary cluster is noted as one of the characteristic features in this approximant.

6.2. $Al_{54}Cu_{25.5}(Fe_{1-x}Ru_x)_{12.5}Si_8$ 1/1–1/1–1/1 *approximants*

The formation of F-type $Al_{54}Cu_{25.5}Ru_{12.5}Si_8$ and $Al_{54}Cu_{25.5}(Fe_{0.5}Ru_{0.5})_{12.5}Si_8$ 1/1–1/1–1/1 approximants with $Pm\bar{3}$ symmetry has been reported (Takeuchi and Mizutani 2001). Chemical disorder is significant in the Mackay icosahedral shell, where 42 atomic positions are occupied by a mixture of 15–25% Al and 75–85% Cu. This chemical disorder in the MI clusters is obviously stronger than that in the P-type 1/1–1/1–1/1 approximant discussed in previous sections. The disorder in the glue sites is more or less the same as that in the P-type approximant. In summary, the F-type 1/1–1/1–1/1 approximant possesses both structural and chemical disorder in the MI clusters and, therefore, the disorder in the F-type 1/1–1/1–1/1 approximants is apparently much stronger than that in the P-type 1/1–1/1–1/1 approximants. Similarly, Sugiyama *et al* (2000) reported that the α-phase Al–Cu–Ru alloy crystallizes into the F-type 1/1–1/1–1/1 approximant with a lattice constant of 12.4 Å and $Pm\bar{3}$ symmetry.

6.2.1. Electronic structure. Roche and Fujiwara (1998) calculated the electronic structure of the F-type Al–Cu–Fe approximant by using a realistic structure of $(Al, Si)_{84}Cu_{36}Fe_{14}$ with 139 atoms in a unit cell determined by Yamada *et al* (1998). The total DOS is found to consist of two peaks: one Cu 3d states at about 5 eV and the other Fe 3d states at about 2.7 eV below the Fermi level. A fairly deep pseudogap is found in the vicinity of the Fermi level with a width of 0.5 eV and the value of DOS at the Fermi level is about 30% of that of pure Al.

The electronic structures of a series of rational approximants to the F-type Al–Pd–Mn quasicrystal have been calculated by Krajcí *et al* (1995), using the *ab initio* pseudopotential, LMTO and tight-binding LMTO techniques. The atomic structure is based on a projection from six-dimensional space with acceptance domain chosen to reproduce the observed diffraction data. They pointed out that a structure-induced minimum in the DOS exists at the Fermi level in the higher-order approximants but is shifted away from it in the lowest-order 1/1–1/1–1/1 approximant, and took this as a characteristic feature of the F-type approximants. It is also emphasized that the s–d hybridization gap at the upper edge of the Mn 3d band enhances the effect due to the Fermi surface–Brillouin zone interaction.

6.2.2. Electron transport properties. As shown in figure 12, the F-type 1/1–1/1–1/1 approximants exhibit a negative temperature dependence of resistivity over a wide temperature range and residual resistivities of 1700–4100 $\mu\Omega$ cm. This is typical of the manifestation of the weak localization. We have pointed out in the previous section the presence of both chemical and structural disorder in the F-type 1/1–1/1–1/1 approximants. This heavily introduced disorder must be responsible for the onset of weak localization, because the weak localization is known to be brought about by multiple elastic scattering due to static disorder.

The resistivity of the $Al_{54}Cu_{25.5}Ru_{12.5}Si_8$ 1/1–1/1–1/1 approximant (3100 $\mu\Omega$ cm at 300 K) is much higher than that of the $Al_{54}Cu_{25.5}Fe_{12.5}Si_8$ 1/1–1/1–1/1 approximant (about 1700 $\mu\Omega$ cm). In the weak-localization regime, the electron mean free path in both cases is certainly limited by an average atomic distance, so the resistivity value should reflect only the electronic structure given by the product of the density of states at the Fermi level and the Fermi velocity (Mizutani 2000). Mizutani (1998) revealed that the resistivity value at 300 K for a large number of quasicrystals increases in proportion to the square of the density of states at the Fermi level in agreement with the Mott conductivity theory. We consider that the electronic specific heat coefficient γ in the former should be much smaller than that in the latter. Indeed, the γ value of the corresponding F-type Al–Cu–Ru quasicrystal is 0.11–0.2 mJ mol^{-1} K^{-2} and is smaller than 0.29 mJ mol^{-1} K^{-2} for the Al–Cu–Fe quasicrystal (Biggs *et al* 1990, 1991). The pseudogap at the Fermi level in Ru-bearing ones must be deeper due to the stronger

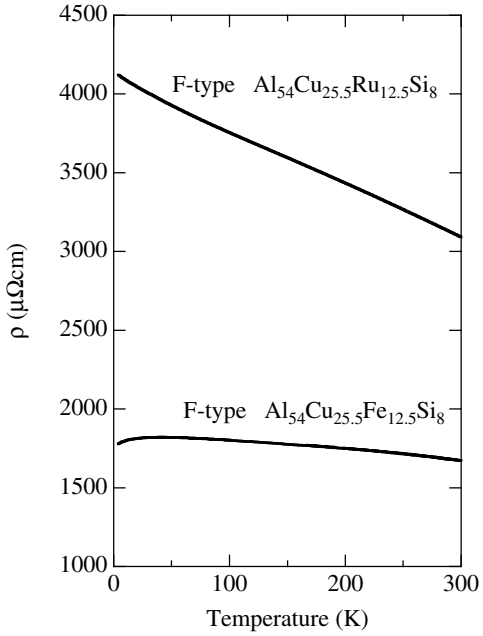

Figure 12. Temperature dependence of electrical resistivity for the F-type $Al_{54}Cu_{25.5}X_{12.5}Si_8$ (X = Fe and Ru) 1/1–1/1–1/1 approximants (Takeuchi and Mizutani 2001).

hybridization effect between the larger TM element Ru and the other elements Al, Cu and Si, and this electronic effect coupled with the chemical and structural disorder contributes to a substantial enhancement in the electrical resistivities.

7. Electron transport properties of other approximants

Before ending the present discussion, it is worthwhile mentioning briefly the resistivity behaviour of approximants in other orders. We noted in section 4.1.3 that the Al–Mg–Zn icosahedral phase possesses the resistivity of 150 $\mu\Omega$ cm, almost three times as large as that of its 1/1–1/1–1/1 approximant. However, in the case of its 2/1–2/1–2/1 approximant, the magnitude of the resistivity was found to be essentially the same as that of the icosahedral phase over a whole temperature range 2–300 K (Takeuchi and Mizutani 1995). Therefore, there exists no difference in the scattering behaviour from the quasicrystal, once the order of the approximant exceeds 2/1 or its lattice constant becomes larger than about 20 Å.

Tamura *et al* (1998) measured the temperature dependence of the electrical resistivity over the range 12–300 K for icosahedral phase and 2/1–2/1–2/1 and 1/0–1/0–1/0 approximants in the Al–Pd–TM (TM = Fe, Ru and Os) alloy system. The resistivity at 300 K ranges from 2000 to 16 000 $\mu\Omega$ cm for Al–Pd–Ru and Al–Pd–Os icosahedral phase, whereas it ranges from 2500 to 7000 $\mu\Omega$ cm for the 2/1–2/1–2/1 approximants. They noted that the temperature dependence of resistivity in the 2/1–2/1–2/1 approximants is almost identical to that of the icosahedral phase. On the other hand, the resistivity at 300 K for the 1/0–1/0–1/0 approximants is smaller than those above and ranges from 400 to 1200 $\mu\Omega$ cm. A negative TCR above about 200 K was accompanied by a resistivity maximum in the temperature dependence of resistivity for the Al–Pd–Fe and Al–Pd–Ru 1/0–1/0–1/0 approximants. This

unique temperature dependence was discussed in terms of the quantum interference effect with strong spin–orbit scattering (Tamura *et al* 2000).

8. Conclusion

We classified 1/1–1/1–1/1 approximants into three groups in terms of the structure type (P or F) and space group ($Im\bar{3}$ or $Pm\bar{3}$) and discussed systematically the electron transport properties on the basis of the experimentally determined atomic structure and the electronic structure calculated for that atomic structure. By making full use of the atomic and electronic structures, we could successfully extract two factors responsible for the phase stability and electrical resistivity behaviour; one arising from the short-range bonding character representing the degree of sp–d hybridization in the atomic cluster and the other the Fermi surface–Brillouin zone interaction representing the long-range order.

In the case of the RT-type Al–Mg–Zn approximant, the long-range order, as reflected in its Fermi surface–Brillouin zone interaction, is solely responsible for the formation of the pseudogap at the Fermi level. The presence of two identical atomic clusters with the space group $Im\bar{3}$ coupled with the validity of the nearly-free-electron model explains well the possession of low resistivities of about 50 $\mu\Omega$ cm or a mean free path much longer than an average atomic distance. An increase in the resistivity value up to 150 $\mu\Omega$ cm in the corresponding quasicrystal can be explained in terms of the long-range order effect, i.e. a reduction in the mean free path due to the destruction of the periodicity of the lattice in the approximant.

On the other hand, the possession of large resistivities exceeding 1500 $\mu\Omega$ cm and manifestation of the weak-localization effect in the F-type approximants in the third group are caused by strong sp–d hybridization in the atomic cluster plus heavily existing chemical and structural disorder in the cluster. Here the mean free path effect is no longer existent. The possession of further larger resistivity in the corresponding quasicrystal must be accounted for in terms of the long-range order effect; a higher multiplicity in the Fermi surface–Brillouin zone interaction in the quasicrystal would naturally yield a smaller density of states at the Fermi level than that in the approximant. This electronic structure effect is most likely responsible for a still existing difference in the magnitude of resistivities between them.

We believe that simultaneous studies of both atomic and electronic structures in diverse families of 1/1–1/1–1/1 approximants would contribute to gaining a deeper insight into comprehensive understanding of the atomic and electronic structures and electron transport mechanism in quasicrystals.

Acknowledgment

One of the authors (UM) wishes to express his deep thanks to Dr E Belin-Ferré for her critical reading of the manuscript and suggesting many valuable comments at the final stage of this study.

References

[1] Belin-Ferré E, Fournée V and Dubois J M 2000 *J. Phys.: Condens. Matter* **12** 8177
[2] Belin-Ferré E, Fournée V and Dubois J M 2001 *Mater. Trans.* **42** 911
[3] Bergman G, Waugh J L T and Pauling L 1957 *Acta Crystallogr.* **10** 254
[4] Biggs B D, Poon S J and Munirathnam N R 1990 *Phys. Rev. Lett.* **65** 2700
[5] Biggs B D, Li Y and Poon S J 1991 *Phys. Rev.* B **43** 8747
[6] Boudard M, de Boissieu M, Janot C, Heger G, Beeli C, Nissen H-U, Vincent H, Ibberson R, Audier M and Dubois J M 1992 *J. Phys.: Condens. Matter* **4** 10 149

[7] Cooper M and Robinson K 1966 *Acta Crystallogr.* **20** 614
[8] Devaud-Rzepski J, Quivy A, Calvayrac Y, Cornier-Quiquandon M and Gratias D 1989 *Phil. Mag.* B **60** 855
[9] Elser V and Henley C L 1985 *Phys. Rev. Lett.* **55** 2883
[10] Fujiwara T 1989 *Phys. Rev.* B **40** 942
[11] Guo J Q, Abe E and Tsai A P 2000 *Phys. Rev.* B **62** R14 605
[12] Guryan C A, Stephens P W, Goldman A I and Gayle F W 1988 *Phys. Rev.* B **37** 8495
[13] Hafner J and Krajcí M 1993 *Phys. Rev.* B **18** 11 795
[14] Hashimoto K, Yamada Y, Yamauchi T, Tanaka T and Matsuda T 1994 *Mater. Sci. Eng.* **A181–2** 785
[15] Henley C L and Elser V 1986 *Phil. Mag.* B **53** L59
[16] Izumi F 1993 *The Rietveld Method* ed R A Young (Oxford: Oxford University Press) ch 15
[17] Janot C 1996 *Phys. Rev.* B **53** 181
[18] Kirihara K, Nakata T, Takata M, Kubota Y, Nishibori E, Kimura K and Sakata M 2000 *Phys. Rev. Lett.* **85** 3468
[19] Koshikawa N, Edagawa K and Takeuchi S 1993 *Mater. Trans. JIM* **34** 188
[20] Krajcí M, Windisch M, Hafner J and Kresse G 1995 *Phys. Rev.* B **51** 17 355
[21] Mizuno T, Takeuchi T and Mizutani U 1999 *MRS Symp. Proc.* vol 553, ed J M Dubois, P A Thiel, A P Tsai and K Urban (Pittsburgh, PA: Materials Research Society) pp 359–64
[22] Mizutani U 1998 *J. Phys.: Condens. Matter* **10** 4609
[23] Mizutani U 2000 *Mater. Sci. Eng.* **294–296** 464
[24] Mizutani U, Iwakami W, Takeuchi T, Sakata M and Takata M 1997 *Phil. Mag.* **76** 349
[25] Mizutani U, Takeuchi T, Banno E, Fourneé V, Takata M and Sato H 2001 *MRS Symp. Proc.* vol 643, ed E Belin-Ferré, P A Thiel, A P Tsai and K Urban (Pittsburgh, PA: Materials Research Society) pp K13.1.1–10
[26] Quivy A, Quiquandon M, Calvayrac Y, Faudot F, Gratias D, Berger C, Brand R A, Simonet V and Hippert F 1996 *J. Phys.: Condens. Matter* **8** 4223
[27] Ramachandrarao P and Sastry G V S 1985 *Pramana* **25** L255
[28] Roche S and Fujiwara T 1998 *Proc. Int. Conf. on Aperiodic Crystals* ed M de Boissieu, R Currat and J-L Verger-Gaugry (Singapore: World Scientific)
[29] Sato H, Takeuchi T and Mizutani U 2001 *Phys. Rev.* B **64** 094207
[30] Shechtman D, Blech I, Gratias D and Cahn J W 1984 *Phys. Rev. Lett.* **53** 1951
[31] Sugiyama K, Kaji N and Hiraga K 1998a *Acta Crystallogr.* C **54** 445
[32] Sugiyama K, Kato T, Ogawa T, Hiraga K and Saito K 2000 *J. Alloys Compounds* **299** 169
[33] Sugiyama K, Kato T, Saito K and Hiraga K 1998b *Phil. Mag. Lett.* **77** 165
[34] Tsai A P, Guo J Q, Abe E, Takakura H and Sato T J 2000 *Nature* **408** 537
[35] Takeuchi T, Banno E, Onogi T, Mizuno T, Sato T, Fourneé V and Mizutani U 2001 *MRS Symp. Proc.* vol 643, ed E Belin-Ferré, P A Thiel, A P Tsai and K Urban (Pittsburgh, PA: Materials Research Society) pp K13.4.1–.6
[36] Takeuchi T and Mizutani U 1995 *Phys. Rev.* B **52** 9300
[37] Takeuchi T and Mizutani U 2001 *Quasicrystals 2001 (Sendai, 2001)*
[38] Takeuchi T, Mizutani U, Yamaguchi S, Fukunaga T, Mizuno T and Tanaka N 1998 *Phys. Rev.* B **58** 11 345
[39] Takeuchi T, Mizuno T, Banno E and Mizutani U 2000 *Mater. Sci. Eng.* **294–296** 522
[40] Takeuchi T, Onogi T, Banno E and Mizutani U 2001 *Mater. Trans.* **42** 933
[41] Takeuchi T, Yamada Y, Fukunaga T and Mizutani U 1994 *Mater. Sci. Eng.* A **181/182** 828–32
[42] Takeuchi T, Yamada H, Takata M, Nakata T, Tanaka N and Mizutani U 2000 *Mater. Sci. Eng.* **294–296** 340
[43] Tamura R, Asano T, Tamura M, Takeuchi S and Shibuya T 1999 *MRS Symp. Proc.* vol 553, ed J M Dubois, P A Thiel, A P Tsai and K Urban (Pittsburgh, PA: Materials Research Society) pp 373–8
[44] Tamura R, Asano T, Tamura M and Takeuchi S 2001 *MRS Symp. Proc.* vol 643, ed E Belin-Ferré, P A Thiel, A P Tsai and K Urban (Pittsburgh, PA: Materials Research Society) pp K13.3.1–6
[45] Tamura R, Komatsu K, Asano T and Takeuchi S 2000 *Mater. Sci. Eng.* **294–296** 607–10
[46] Trambly de Laissardiére G, Nguyen Manh D, Magaud L, Julien J P, Cyrot-Lackmann F and Mayou D 1995 *Phys. Rev.* B **52** 7920
[47] Tsai A P, Inoue A and Masumoto T 1987 *Japan. J. Appl. Phys.* **26** L1505
[48] Yamada H, Iwakami W, Takeuchi T, Mizutani U, Takata M, Yamaguchi S and Matsuda T 1997 *Proc. 6th Int. Conf. on Quasicrystals (Tokyo, 1997)* ed S Takeuchi and T Fujiwara p 664
[49] Yamada H, Takeuchi T, Mizutani U and Tanaka N 1999 *MRS Symp. Proc.* vol 553, ed J M Dubois, P A Thiel, A P Tsai and K Urban (Pittsburgh, PA: Materials Research Society) pp 117–22
[50] Yamamoto A 1996 *Acta Crystallogr.* A **52** 509